Zentrum für Technomathematik
Fachbereich 3 – Mathematik und Informatik

Mathematical Optimization of Simulated Laser Welds Mathematical Optimization of Simulated Laser Welds on Aluminum Alloys

Jonathan Montalvo-Urquizo
Alfred Schmidt

Report 08–04

Berichte aus der Technomathematik

Report 08–04 November 2008

Mathematical Optimization of Simulated Laser Welds on Aluminum Alloys

J. Montalvo-Urquizo[a,*], A. Schmidt[a]

[a] *Zentrum für Technomathematik, Fachbereich 3, University of Bremen, Germany*

Abstract

We present a coupled simulation–optimization procedure for the improvement of the laser welding process. This is achieved by introducing a functional to measure the quality of a weld and later performing a mathematical optimization of it. The welding process to be included in the functional is simulated using an adaptive finite element method for the thermal and mechanical subproblems. The functional is optimized using a constrained mathematical optimization method and the optimized parameters giving some desired properties of the welds are found.

In this paper, the results obtained for two different optimization goals are presented, namely a general test problem in which all good properties of the welds are assumed to have the same importance, and another in which a higher importance is given to the residual stress and the full penetration of the weld.

Key words: welding, laser welding
PACS: 44.05.+e, 46.35.+z, 81.20.Vj

1. Introduction

The precise calibration of a process represents one of the most common practical problems in industrial applications, and thus the search for adequate parameters is an important task before a process can be implemented in the production lines. The complexity of such calibration depends strongly on the process complexity and is some times done by large and expensive experimental tests.

[*] Corresponding author
Email addresses: montalvo@math.uni-bremen.de (J. Montalvo-Urquizo), schmidt@math.uni-bremen.de (A. Schmidt)

For the welding community, the main interest is to analyze the properties of the welded pieces, mainly observing the seam construction and the possible mechanical distortions that the pieces could contain, i.e. evaluating the weld seam geometry and the residual stresses and deformation.

The laser welding process contains a complex relation that traduces some basic process parameters like laser intensity and process velocity, into the resulting welded products. A calibration of a process using a slightly different material or laser array requires in many cases an expensive (and some times unavailable) working cycle in which sample welds are produced, measured for resulting distortions and/or stresses, and then cut for measuring the weld seam dimensions and the quality of the weld.

Although this calibration cycle is usually guided by already existent know-how for similar processes, the calibration remains expensive and is only able to find, among the performed process trials, the one that results in the better outputs.

The driving idea in this work is to embed the laser welding process inside a functional that can measure the quality of a welded product. This will allow the use of the existent mathematical optimization theories and algorithms to find the optimal parameters producing the best welds.

Some previous works in which an optimization in the mathematical sense has been applied to the welding problem already exist. For example, the works in [1, 2] are based in quasi-stationary analytical solutions for the temperature field and a simple model is used to predict hot-cracks. This is later included in an optimization procedure to eliminate the appearance of hot-cracks in the welded pieces.

The computational welds we consider have a higher level of complexity and the intended optimization has different goals, as will be shown in the model description in the forthcoming Section 2. The optimization setting and method are explained in Section 3, and Sections 4 and 5 present two different optimization results, showing the flexibility of the implemented ideas for the quality of the welds. Finally, section 6 presents the final remarks and outlook of this work.

2. Mathematical Model and Simulation

We consider here the laser welding process as in [3, 4], where the complete mathematical model and their calibration with experimental results were presented. All the simulated processes make are Adaptive FEM implementations that make use of the open source toolbox ALBERTA ([5]).

2.1. Thermal model

The material pieces are described by the domain Ω (assuming that there is no gap between them) and a modified heat equation is solved for the temperature θ, it is

$$\frac{\partial \theta}{\partial t} - \frac{\partial}{\partial x}\left(\kappa(\theta)\frac{\partial \theta}{\partial x}\right) = 0 \qquad \text{in } \tilde{\Omega} \times (0, T), \tag{1}$$

$$\kappa(\theta)\frac{\partial \theta}{\partial n} = \delta_{air}(\theta - \theta_0) \qquad \text{on } \partial\Omega \times (0, T), \tag{2}$$

$$\theta = \theta_0 \qquad \text{in } \tilde{\Omega} \times \{0\}, \tag{3}$$

$$\theta = \theta_v \qquad \text{in } \Omega \backslash \tilde{\Omega}, \tag{4}$$

where $\kappa(\theta)$ is the temperature dependent heat diffusivity, δ_{air} is the heat transfer coefficient from the material pieces to the surrounding air, and the room and evaporation temperature are denoted by θ_0 and θ_v, respectively. Further, the subdomain $\Omega \backslash \bar{\Omega}$ is determined by the vapor channel or keyhole shape obtained with the models in [6, 7].

In [3, 8], the use of this modified equation has been shown to give good results in accordance with experiments.

Figure 1 shows the specific geometry used for the simulations, with a total dimensions of 100mm $\times$ 65mm $\times$ 3mm. The beam is assumed to be moved along the middle line of the plates, producing a keyhole moving in the interval $x \in [15\text{mm}, 85\text{mm}]$.

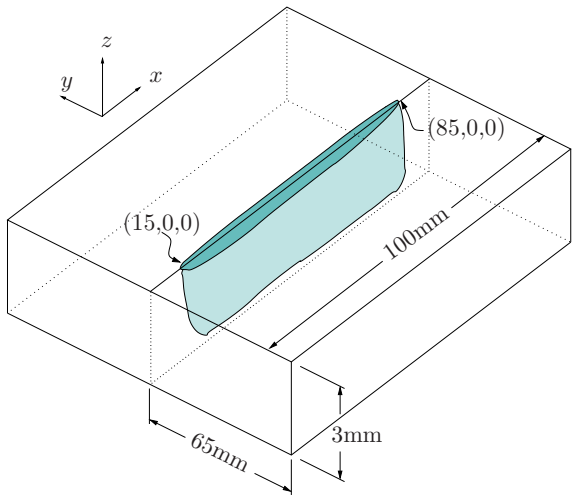

Figure 1: Material piece geometry with start and end points for the butt-weld.

Figure 2 shows a simulated temperature field for the specified geometry, where the temperatures above the melting temperature of 650°C are colored in red and it is possible to observe the characteristic shape of the temperature distribution for a welding process.

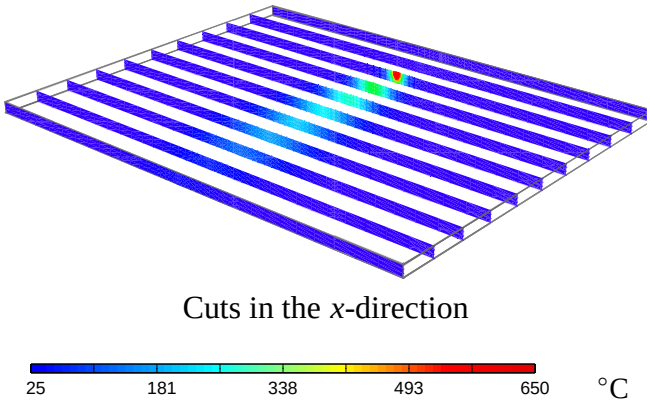

Figure 2: Temperature field at $t = 0.88$ s. Temperatures above the melting point are omitted.

This simulation result corresponds to a value of laser power of 3000W, a welding velocity of 75mm/s, and was performed using the set of temperature-dependent material properties for the aluminum alloy AA6082-T6 as in the appendix A of [3].

More extended simulation thermal results can be found in [3, 4, 8], where also several comparisons with experimental measurements in the welds are presented.

2.2. Mechanical model

Based in the temperature fields, the corresponding elasto–plastic problem is solved using the radial return mapping as in [3]. The algorithm used performs an update of the deformation field $u(x)$, the strain tensors $\varepsilon(x)$ and the stress tensors $\sigma(x)$, making use of a predictor–corrector procedure to give stress tensors that are inside the set of allowable stresses.

The use of a model which includes plastic deformations allows the calculation of the residual state of the piece, making possible the measurement of the distortion in the pieces after the material has cooled down. This residual state is a very important ingredient for the optimization aims, as the final stresses and distortions are an important part on the quality of a welded product.

Within this work, the mechanical calculations assume a flow rule with isotropic linear hardening (see e.g. [9, 10]) and von Mises yield criterion (as in [3, 4]).

The core of the plastic solver is the predictor-corrector step performed in each quadrature point of the FEM simulation at each time-step and consists on the evaluation of the stress using the linear elasticity model as predictor and, if necessary, a correction to avoid the current stress to be outside the level which can be loaded into the material. For more details, see the general algorithms in [9] or the specific algorithm used in [4].

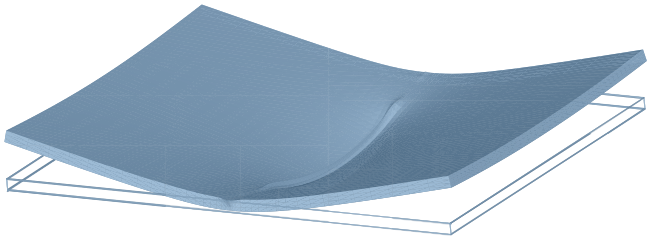

Figure 3: Final deformation of the butt welded piece. Exaggerated 30 times and measured after 300 seconds of cooling have passed since the welding procedure has finished.

Figure 3 shows the result for the final distortion or deformation of the welded plates. The deformation shown here corresponds to the cold material piece and makes possible to observe the typical deformation obtained in practice for such a welded piece ([11, 12]).

This shape of the welded piece is created due to the different thermal distributions obtained for different vertical layers on the pieces, causing that the thermal effects differ and finally the internal stresses cause this bending/folding effect in the plates.

3. Optimization method and settings

3.1. Functional for the weld quality

For a real (or simulated) process to be optimized, a crucial point is the selection of the objective function, as it must be the 'measure' of any element or the possible process results. In particular, for the laser welding application, the function $F(x)$ should be understood as a measure of *quality* or *goodness* of the welds, while the argument x must be a vector holding the possible inputs to create one of them, either by real welding or, as in our case, by simulating it numerically.

First of all, we set our problem as the mathematical optimization problem

$$\min_{x \in \mathbb{R}^n} F(x), \quad l \leq x \leq u, \tag{5}$$

where the inequalities are assumed to work componentwise and fulfill $l_i < u_i \ \forall i$. In this work we assume that the functional has the form

$$F(x) = \sum_{j=1}^{m} \frac{\alpha_j}{2} \left\| f_j(x) \right\|^2, \tag{6}$$

where $x = (x_1, x_2, \ldots, x_n)^T$ is the vector including the n input parameters for the objective function.

Considering functions of this type, we can write an equivalent form for F as

$$F(x) = \frac{1}{2} f(x)^T f(x), \tag{7}$$

with

$$f(x) = \begin{pmatrix} \sqrt{\alpha_1}\, f_1(x) \\ \sqrt{\alpha_2}\, f_2(x) \\ \vdots \\ \sqrt{\alpha_m}\, f_m(x) \end{pmatrix} \in \mathbb{R}^m. \tag{8}$$

Using the representation (7), the functional's gradient is

$$\nabla F(x) = J^T(x) f(x) \in \mathbb{R}^n, \tag{9}$$

where $J_f(x) \in \mathbb{R}^{m \times n}$ denotes the Jacobian matrix of the vector $f(x)$. This simple form of ∇F makes the quadratic function (7) a very convenient setting for practical optimization tasks. Furthermore, in problems of parameter identification type with well established desired values, this kind of functions arise in a natural way.

What is not trivial to show in an applied problem, is the sufficient regularity of the functional F, as it normally involves many interrelations among the physical parameters.

In the case of laser welding, the regularity of the functional can not be easily established, as it depends on a complete chain of interrelations, going from the energy impigned into the material through the keyhole formation and its use as moving heat source, to the retrieval of the temperature fields. This, together with the fact that all physical parameters present regularity problems around the melting temperature, makes very difficult to obtain theoretical results about the regularity of F. A further discussion on this topic can be found in [3].

The idea now is to construct a function as the one in (7) to represent the welds in a way that the good and bad states of certain properties can be quantitatively represented, making use of the most important features of the process.

Due to the complexity of the laser welding process, it is impossible in practice to include a large amount of parameters for an optimization procedure. For this reason, we only consider the main inputs of the process as arguments of the objective function, namely the laser power impinged to the material (P) and the process velocity (v). Furthermore, we also assume that the thermal/mechanical initial and boundary conditions are known and equal for all welds.

Apart from the selection of the inputs, the objective function must measure the goodness of different welds, considering the simulated versions of a real weld evaluation.

The features that we consider to evaluate a real or simulated weld are the economy and efficiency of the process, the residual deformations in the pieces, and the shape of the weld seam. By economy of the process, we understand the use of laser power in a low range. Inside the process efficiency, we include the process velocity and the use of only the necessary amount of laser beam power.

The weld features to be observed contain complex interrelations, and the improvement on some of them could lead either to improvements or degradations in the others. For example, the use of lower laser power and welding velocity produce lower deformations, but this also produces very wide weld seams, which is traduced in lack of strength of the final piece over a larger volume. Some other examples of this kind of interrelations can be found in [3].

Our selection of input parameters for the welds can be extended in a straightforward manner. The only big disadvantage is the direct increase in the computational effort to evaluate every iteration of the search, due to the dimension growth of the Jacobian, as this is approximated using a finite differences scheme.

We shall consider a functional of the form (7), with the vector of laser power and velocity as inputs

$$x = \begin{pmatrix} P \\ v \end{pmatrix} \tag{10}$$

and the components of $f(x)$ as

$$f_1(P, v) = \sqrt{\alpha_1}\ (P - P_D)\,, \tag{11}$$

$$f_2(P, v) = \sqrt{\alpha_2}\ (v - v_D)\,, \tag{12}$$

$$f_3(P, v) = \sqrt{\alpha_3}\ (w - w_D)\,, \tag{13}$$

$$f_4(P, v) = \sqrt{\alpha_4}\ (h - h_D)\,, \tag{14}$$

$$f_5(P, v) = \sqrt{\alpha_5}\ (s)\,, \tag{15}$$

where w, h, s denote the width of the weld seam, its height, and the measure of residual stress in the material, respectively, and the subscript D denotes *desired values* of the same variables.

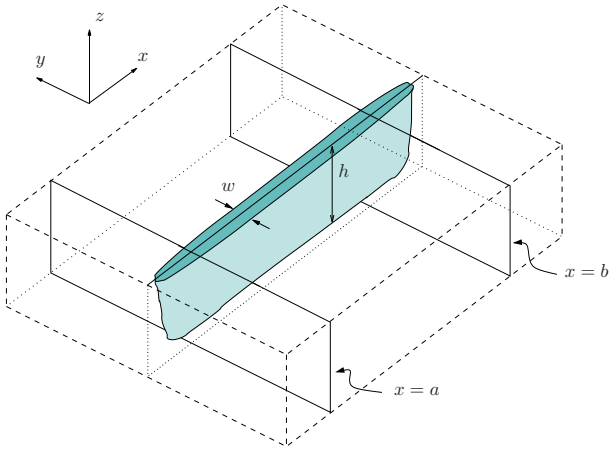

Figure 4: Stable domain for the weld evaluation. The evaluation region is defined as the points with $x \in [a, b]$.

The values of w, h and s are determined only in a subdomain of the welded piece in order to avoid the unstable initial and ending points of the process (see [3] for more details). The subdomain depicted in Figure 4 was used in our algorithms with $a = 30$mm and $b = 70$mm.

Averaging all the melting pools dimensions inside the stable subdomain gives the values of w and h. The value s describes the residual deformation in the welded piece and in our algorithms can be selected as the equivalent stress or as the out-of-plane angle.

From this setting, it is clear that the practical problem is bounded by the practical values of the inputs, as

$$\begin{array}{rcccl} 0 < P_{min} & \leq & P & \leq & P_{max} < \infty, \\ 0 < v_{min} & \leq & v & \leq & v_{max} < \infty. \end{array} \tag{16}$$

and the practical process indicates directly our desired values for this parameters, it is $P_D = P_{min}$ and $v_D = v_{max}$.

The desired values for the weld seam geometry are positive numbers and the desired height can be naturally considered as the material thickness.

The stress measurement is presented without desired value in equation (15) because the best possible solution would be a weld presenting no residual stresses or deformations.[1]

[1] Although this not possible in practice, the use of zero as desired value does not represent any trouble for the mathematical optimization.

The measurement of stress in (15) can be considered as a norm of the stress over the whole piece. Normally, equivalent stresses are considered for this measure. However, there can be other ways to include this feature in the functional, as the ones presented in [3].

3.2. Constrained optimization method

Within this work, we solve the constrained optimization problem in (5) by the interior trust region method in [13, 14] which is based in the previous works [15, 16, 17, 18] and corresponds the base of the constrained optimization used in [19].

The method presented in [15, 16, 17, 18] is mainly based on an affine scaling of the problem that forces the iterations to belong to the interior of the bounds. This scaling is performed by defining the vector function $v : \mathbb{R}^n \to \mathbb{R}^n$ defined componentwise as

$$v_i(x) = \begin{cases} x_i - u_i & \text{if } g_i < 0 \text{ and } u_i < \infty, \\ x_i - l_i & \text{if } g_i \geq 0 \text{ and } l_i > \infty, \\ -1 & \text{if } g_i < 0 \text{ and } u_i = \infty, \\ 1 & \text{if } g_i \geq 0 \text{ and } l_i = \infty. \end{cases} \tag{17}$$

and the scaling matrix D for an iteration point $x^{(k)}$ as

$$D(x^{(k)}) = \text{diag}(\left|v(x^{(k)}\right|^{-\frac{1}{2}}). \tag{18}$$

With this definitions, the first order optimality conditions can be written as the nonlinear system of equations

$$D(x)^{-2} g(x) = 0. \tag{19}$$

The further development of this method produced the STIR method in [13, 14], which maintains all the good convergence properties and features shown in [17, 18], but is also able to deal with large scale problems. The base to handle with the large scale problems is a subspace idea using a preconditioned conjugate gradient procedure. For a short overview of the methods development and their main ideas, the reader is referred to [3]. The main features of the STIR method are:

- use of the affine scaling to only allow iterations inside the bounds;
- adaptive trust region size, considering the distance to the bounds, the decrease on the function, and the good approximation of a quadratic submodel to the original functional; and

- each iteration is taken as the best solution between the subspace-based solution from [14], the reflected-path solution from [16] and the solution along the negative gradient direction.

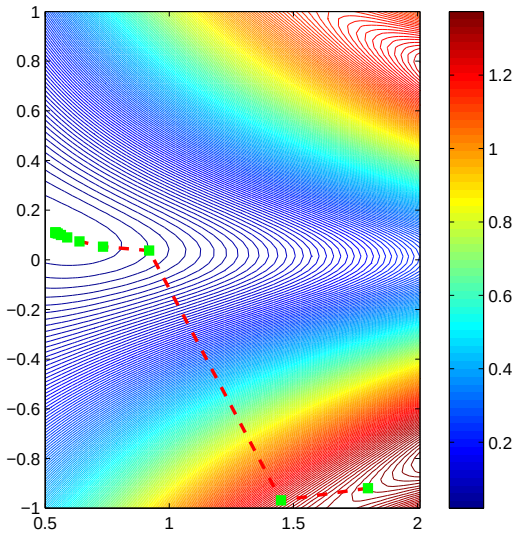

Figure 5: Iterative solution search using different starting points for a box constrained example with a reflective Newton method.

As an example, Figure 5 shows the performance of the method for the minimization of the function

$$F\begin{pmatrix} x_1 \\ x_2 \end{pmatrix} = \frac{1}{6}\left(\|2\sin(x_1 x_2)\|^2 + \|(x_1 - 0.6)\|^2 + \|(x_2 - 0.4)\|^2\right) \qquad (20)$$

with the bounds $0.5 \leq x_1 \leq 2$ and $-1 \leq x_2 \leq 1$ and with the starting point $x^{(0)} = (1.8, -0.9)^T$.

For this test example, it is worth to notice from the isolines how the function forces the first iteration, $x^{(1)}$, to point outside the restricted domain, but the lower bound for x_2 is never crossed. Later, the step to obtain $x^{(2)}$ is much larger than the previous one, indicating that the trust region size was increased in this iteration. Finally, the convergence towards a minimum can be observed, taking smaller steps until the minimum step-tolerance is reached.

The STIR method was implemented as a C-library, using the algorithms and tolerances as described in [3]. Further, the simulation presented in Section 2 was used three times for each iteration, due to the necessity to evaluate the current

point $x^{(i)} = \left(P^{(i)}, v^{(i)}\right)$ and two more neighboring points for the evaluation of the gradient, i.e. $\left(P^{(i)} + \Delta P, v^{(i)}\right)$ and $\left(P^{(i)}, v^{(i)} + \Delta v\right)$.

In the next sections, we assume that the simulated welding process from Section 2 has been already calibrated (as in [4]) and do not distinguish between a weld and its correspondent simulation. For simplicity, the next sections omit the use of units, unless they are needed for the analysis.

4. Optimization without special weighting

This section presents a first optimization procedure in which we assume that all the factors in the subfunctions $f_1, \ldots, f_4$ have the same importance, while the mechanical result in f_5 is totally neglected.

The driving idea of every factor in the objective function having the same importance may not be of high practical interest and should not be understood as a proposal for real applications. It only tries to give an insight of the general optimization runs over a rather simple setting that might not be easy to understand on a more realistic optimization. The mechanical result is neglected in this first optimization to avoid the computations of this submodel, and to allow the optimization to be done using pure thermal simulations.

Recalling the minimization setting for the functional F as in equation (7), with the sufunctionals given as in equations (11)–(15), the optimization problem is fully determined by the desired values, the weights for each component of F and the bounds to which the inputs of the objective function must be restricted.

	P	v	w	h
Desired value	2000	140	2.5	−3.0
Weight α_j	1000	1000	100	100

Table 1: Desired values and corresponding weights.

The desired values and weights for the simulations in this section are shown in Table 1, and the bounded domain is defined trough the practical limits in the laser power and the usual process velocities as

$$1000 \leq P \leq 6000, \tag{21}$$

$$40 \leq v \leq 150. \tag{22}$$

The weights α_j were selected considering the typical values obtained from the simulations, in a way that the multiplication of the terms of the form $\alpha_j \| f_j \|^2/2$

	OPT-Ia	OPT-Ib	OPT-Ic	OPT-Id	OPT-Ie
$P^{(0)}$	1050	2000	5400	5500	5900
$v^{(0)}$	50	60	42	80	135

Table 2: Different starting points for the optimization procedure.

would lead to values of the same order. This weighting idea mimics a process in which all the four sub-functionals have the same importance and the corresponding optimization search will try to improve every factor in the same manner.

Although the weights for the laser power and velocity components seem to be very high when compared to the other weights, it must be said that these variables correspond to the inputs of the objective function, and their values are scaled to belong to the unit square (see [3] for details). The same scaling is done for the corresponding desired values.

The optimization runs are performed using the implementation of Algorithm 9 in [3]. For all the optimization runs, the main constants and stoping criteria for the implementations were taken as:

Iterations

Maximum number of iterations: 20
Maximum function evaluations: 60

Stoping criteria

Minimum step size: 10^{-3}
Minimum function decrease: 10^{-4}
Allowed distance to bounds: 10^{-4}

In order to analyze the performance of the optimization search, we started the optimization from the five initial points in Table 2, each of them with the label "OPT-I" and an extra lower case letter. These points belong to different regions of the admissible domain and will give an idea of the functional shape and the existence of a minimum. Figure 6 shows the different search paths obtained with these points, leading to final results in the same region. The values of the objective function at the starting and final points are presented in Table 3, where also the values of the resulting weld seam are presented.

The search stops in all cases due to non sufficient decrease of the objective function along the search directions and, at the same time, the objective function values at the different final values (F_{end}) are rather similar.

As all the search directions point at some time to the interior of the non reached zone, the only explanation for this mismatching could be that the objective func-

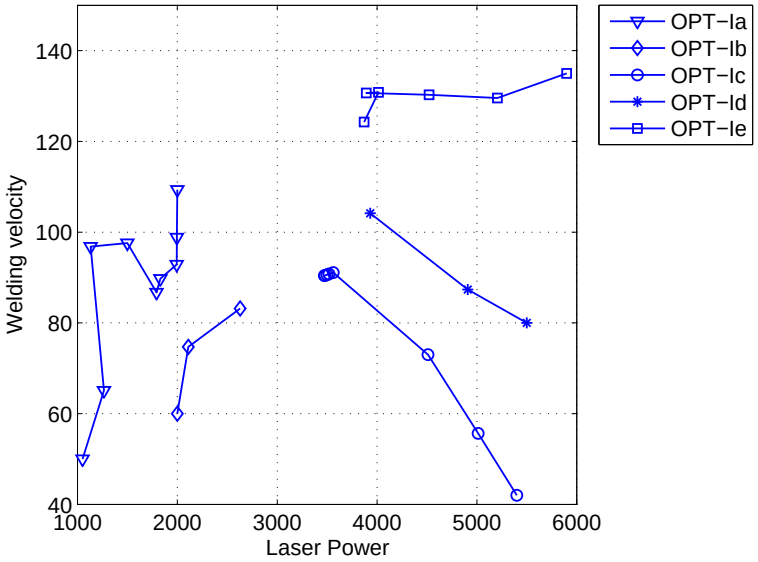

Figure 6: Optimization search paths for different starting points.

tion has a flat valley in the region inside the final iterations. Figure 7 presents an interpolation of all computed values of the objective functions through the five optimization procedures. It is important to mention that, among the considered points for the interpolation, there are many of them belonging to the interior of the apparent flat valley. These points are the result of the simulations done during the finite difference approximation to the Jacobian of the function at each iteration point.

From the results in Table 3, the iteration number does not necessarily fit with the iterations which can be observed in the search path of Figure 6. There can be missing iteration points in the paths because some of the iterations could have been rejected during the search process, due to bad approximation of te functional through the trust region submodel (see e.g. [20, 13]).

The rejection of an iteration as part of the function-decreasing path is then followed by a reduction of the trust region size at the last decreasing point, and a restart of the search from this last decreasing point. The change in the trust region size corresponds to the reduction or enlargement indicated in Algorithm 10 in [3].

As an example for the accepted and rejected points, Table 4 contains the complete iteration points for the OPT-Id, together with their objective function values

	OPT-Ia	OPT-Ib	OPT-Ic	OPT-Id	OPT-Ie
F_0	1035.69	695.40	1673.12	787.65	733.24
F_{end}	492.13	453.97	417.80	438.93	384.39
P_{end}	1999.99	2629.02	3471.84	3931.81	3871.10
v_{end}	109.36	83.17	90.41	104.18	124.29
w_{end}	1.706	2.113	2.113	1.977	1.909
h_{end}	−1.125	−1.750	−1.938	−1.750	−1.625
Iterations	14	8	14	9	10
Simulations	42	24	42	27	30

Table 3: Initial an final values of the objective functions, and values of the final parameters and their corresponding results of weld seam geometries.

Iteration	P	v	$F(P,v)$	Accepted	Trust region size
x_0	5500.000	80.000	787.646	✓	initial
x_1	4909.516	87.344	582.977	✓	maintained
x_2	3931.222	104.162	440.725	✓	maintained
x_3	4318.391	121.617	466.872	×	reduced
x_4	4062.835	108.056	445.677	×	reduced
x_5	3967.422	105.077	446.761	×	reduced
x_6	3940.494	104.386	440.836	×	reduced
x_7	3933.554	104.218	440.755	×	reduced
x_8	3931.806	104.176	438.934	✓	maintained

Table 4: Iterations for the optimization OPT-Id, with value of the objective function.

and the change they produce in the trust region size. Additionally, the points in Figure 8 show the accepted points (circled) and the rejected points (crossed) for the same optimization run.

Although the observable circled points are only three, it is important to notice that they correspond to the iterations x_0, x_1, x_2 and x_8, but the last two of them lie in very close locations and are undistinguishable in the plot. In this plot, it can be observed how the iterative search overestimates the goodness of the approximation after finding x_2, and starts a search over a large trust region, deriving in x_3.

At x_3 the method finds the minimum on the approximated quadratic model, but it results in an increase of the value of the original objective function and the point has to be rejected. After this, the points x_4, x_5, x_6 and x_7 present the same

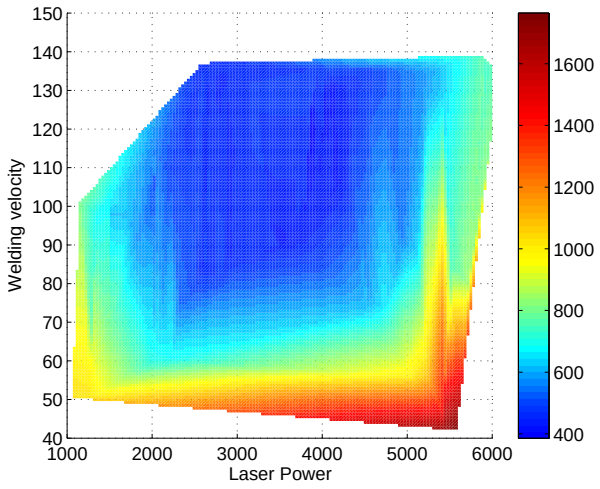

Figure 7: Interpolated objective function.

problematic and are rejected as well, deriving in a reduction by a factor of 0.25, which is predefined in the implementation of Algorithm 9 from [3].

Finally, when the last reduction is done, the point x_8 slightly reduces the objective function, but the size of the step is of 0.584 W and 0.014 mm/s. After being scaled to the unit square, the size of this step falls below 10^{-3}, which is the minimum step size tolerance given to the program. In a practical sense, it can also be said that this step does not represent any significant size and the iterations x_2 and x_8 can be seen as equivalent.

Considering again the five optimizations OPT-Ia through OPT-Ie, it can be mentioned that each of them produces an approximation to the flat region from a different side, and they are all optimal in a different sense. It is observable, for example, how OPT-Ia improves very well the laser power value (P), but does not care about the bad values for the weld seam geometry. In the other hand, OPT-Ic results in the best obtained weld seam geometry, but the laser power and velocity of the process are far from their desired values.

In the following section, we present an optimization with more similarity to the real welding processes, and where the different parts in the functional have specific importance and the large flat valleys in the objective function does not appear.

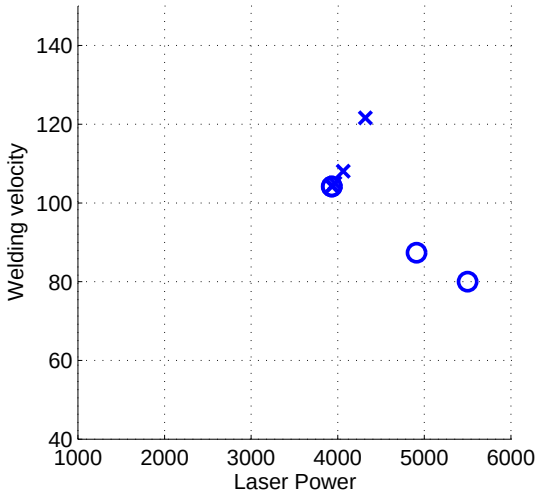

Figure 8: Accepted (○) and rejected (×) points for the OPT-Id.

5. Optimization of residual stress and welding penetration

In this section we also consider the mechanical effects occurring in the material and we focus our optimization goals in the small residual stress and the full penetration of the weld.

For the measurement of the stress we use only the stable subdomain with $x \in [30,\ 70]$, as in Figure 4. This selection is based on the known stable behavior of the stress in the middle of the weld, being not influenced by either the extremes of the weld seam, or the longitudinal boundaries. Inside this domain, the equivalent stress is smooth and maintain its shape along the welding direction. The other dimensions are completely included in the evaluation, it is $y \in [-65,\ 65]$ and $z \in [-3,\ 0]$ and we use the L^2 norm of the equivalent stress divided by the volume of the resulting subdomain.

In order to maintain the search focused, we search for our optimal weld with a very realistic idea in practice. For this, we require that the welded piece is fully penetrated, and the residual mechanical effects on it must be as small as possible. Furthermore, from these two main goals, the full penetration of the weld should be put in the first place.

We also consider the energy consumption and the process velocity in the optimization, but with a much smaller importance level. The values of the weld seam width are not considered at all in this optimization. With this, the desired values and corresponding weights are selected as in Table 5

	P	v	h	$\|\sigma_{eq}\|$
Desired value	1000	150	-3.0	0
Weight α_j	100	100	5000	3000

Table 5: Desired values and corresponding weights.

Using this weighting for the weld evaluations, the optimization search corresponds to an optimization process very close to what is needed in the practical welding community, as the search tries to find the parameters for a fully welded product with small distorted areas, and without totally forgetting the low energy consumption and the time used to create the welds.

With the weights selected as in Table 5 and the similar values for the optimization in the previous section, it can be observed that the value of the penetration subfunctional is now considered to be 500 times more important than the laser power and the velocity, and the residual stress norm is also considered 300 times as important as these values. Additionally, neglecting any importance of the weld seam width does not represent a big problem, as we assumed the perfect attachment of the two plates, leaving no gap between the two pieces.

The points of the search are presented in Table 6, where also the values of the objective function and the obtained measure of stress are presented.

Iteration	P	v	h	$\|\sigma_{eq}\|$	$F(x)$	Accepted
0	5590.00	80.00	-3.04	0.677	593.31	✓
1	5614.60	93.15	-3.00	0.618	493.50	✓
2	4451.11	107.15	-2.19	0.576	3707.36	×
3	5315.99	96.47	-3.00	0.617	479.12	✓
4	4967.59	96.52	-2.67	0.621	1008.60	×
5	5228.92	96.51	-3.00	0.619	477.80	✓
6	5142.74	96.56	-3.00	0.616	471.52	✓
7	4972.08	96.59	-2.67	0.624	1014.55	×
8	5100.13	96.59	-2.67	0.624	1018.20	×
9	5132.21	96.58	-3.00	0.612	466.41	✓
10	5111.02	96.62	-2.67	0.626	1015.01	×
11	5127.11	96.61	-2.67	0.623	1015.64	×
12	5131.06	96.60	-3.00	0.609	463.22	✓

Table 6: Iterations for the full penetration and low residuals stress optimization.

It is necessary to mention that for cases in which the vertical keyhole dimension is higher than the material thickness, this number is used as value for h. With this, the optimization would also find points (P, v) for which only the necessary energy expense is done.

In Table 6 can be observed how a common feature of the rejected points is that the penetration of the weld is not complete. It is interesting that the point x_2 has the smallest equivalent stress but it is rejected due to its small penetration value.

The accepted points of the search are shown in Figure 9, where a zoom of the admissible domain was chosen in order to have a closer impression of the search performed.

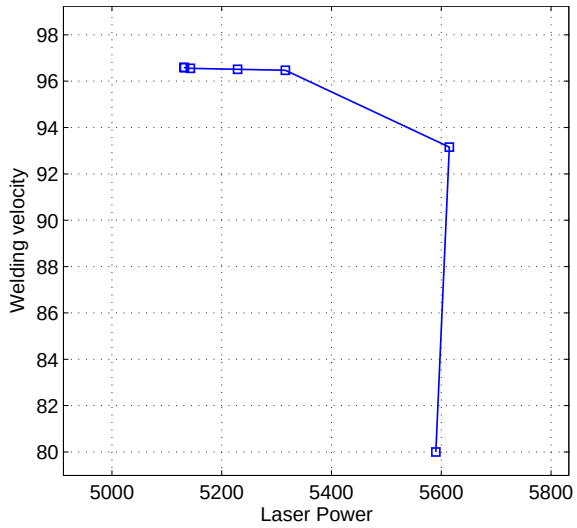

Figure 9: Search for the optimal values giving full penetration and the minimal stress affected zone. Only a subdomain of the admissible set is shown.

Making a short summary of this optimization run, it can be mentioned that the laser power was improved by 459 W (8%), the velocity is improved by 16.6 mm/s (21%), the final weld is full penetrated, and the norm of the equivalent stress in the selected subregion is decreased by 10%.

In words, the welds using the process parameters found by the optimization search will contain less residual stress (and thus less distortion) while staying fully welded, and at the same time the process will be more economical and will be produced considerably faster.

6. Discussion and future research

Using our previous works described in [3, 4], we have presented here a successful optimization procedure for the laser welding process. The optimizations presented here, together with other ones in [3, 8] show the flexibility of the method used here and its simple use for diverse optimization goals.

Particularly, the optimization procedure in Section 5 has shown that the implemented procedures are suitable to work in realistic optimization tasks, not only achieving the desired features in the welded products, but also improving the efficiency and economy of their production.

It is clear that the simulation and optimization loops including the mechanical computations are not as fast as the thermal ones. However, the virtual process can be done without the necessity of having a real workshop to create the welds, by simply using a PC to compute the simulations and the optimal values. With a correctly calibrated simulation system, the simulation-optimization loop is much more convenient than any systematic search using real welds, as its costs are negligible when compared to the possible analysis costs over real welded pieces.

Although the STIR method from Section 3 gives good results and other authors have proved its comparable performance to other methods based on active set type, the optimization of welding has only been done with this method, and the performance of other optimization procedures is unknown until now. This is an open possibility that can be followed in our future research.

Finally, it is important to remember that the optimization method here presented is general and the use of only two input variables is a special case. Objective functions including more input variables or other factors to evaluate the welds are also supported by the implemented optimization procedures.

The results of this work are very promising and indicate that the procedure could also work in a real industrial application, or in the optimization of other complex physical models. Additionally, the implemented optimization can be slightly modified to work with similar problems, in which a simulation tool already exists.

The use of extended optimization functionals can also be considered for future research. Some first extension and modification ideas have been already proposed in [3], but many others can be also considered.

Acknowledgements

The authors thank to the ZF of the Universität Bremen and to the CONACYT-Mexico for the financial Support.

References

[1] V. Petzet, C. Büskens, H. J. Pesch, V. Karkhin, M. Makhutin, A. Prikhodovsky, V. Ploshikhin, OPTILAS: Numerical Optimization as a Key Tool for the Improvement of Advanced Multi-Beam Laser Welding Techniques, in: A. Bode, F. Durst (Eds.), High Performance Computing in Science and Engineering: Transaction of the KONWIHR Result Workshop, Springer, 2005, pp. 153–166.

[2] V. Petzet, C. Büskens, H. J. Pesch, A. Prikhodovsky, V. Ploshikhin, Different optimization models for crack-free laser welding, Proc. Appl. Math. Mech. 5 (1) (2005) 755–756.

[3] J. Montalvo-Urquizo, Simulation and Optimization of Laser Welding on Aluminum Alloys, Ingenieurwissenschaften, Dr Hut Verlag, München, 2008.

[4] J. Montalvo-Urquizo, Z. Akbay, A. Shmidt, T. Pretorius, Adaptive Finite Element Models Applied to the Laser Welding Problem, Berichte aus der Technomathematik 08-03, Zentrum für Technomathematik, Universität Bremen (2008).

[5] A. Schmidt, K. G. Siebert, Design of Adaptive Finite Element Software: The Finite Element Toolbox ALBERTA, Springer, 2005.

[6] W. Jüptner, T. Kreis, Mathematisches Model zur Beschreibung der Wechselwirkung zwischen Strahlen hoher Intensität und technischen Werkstoffen, Forschungsbericht, Bremer Institut für angewandte Strahltechnik (1982).

[7] R. Rothe, Beispielsrechnung für konstante, gaussförmige und ringförmige Verteilung der Leistungsdicht für gleiche Parameter, unpublished.

[8] Z. Akbay, J. Montalvo-Urquizo, T. Pretorius, F. Vollertsen, Fast FEM-Model and Keyhole-Heat Source Model for Self-Optimized Simulation of Laser Welding Processes, in: F. Vollertsen, J. Sakkiettibutra (Eds.), Thermal Forming and Welding Distortion: Proceedings of the International Workshop on Thermal Forming and Welding Distortion, BIAS, 2008, pp. 277–288.

[9] J. C. Simo, T. J. R. Huges, Computational Inelasticity, Springer, 1999.

[10] W. Han, B. D. Reddy, Plasticity: Mathematical theory and numerical analysis, Springer, 1999.

[11] U. Dilthey, Schweisstechnische Fertigungsverfahren, 3rd Edition, Vol. 2: Verhalten der Werkstoffe beim Schweissen, Springer, 2005.

[12] F. Vollertsen, G. Habedank, Schweisstechnische und verwandte Verfahren 1, Lecture notes, University of Bremen (2004).

[13] M. A. Branch, Inexact Reflective Newton Methods for Large-Scale Optimization Subject to Bound Constraints, Ph.D. thesis, Cornell University (January 1996).

[14] M. A. Branch, T. F. Coleman, Y. Li, A Subspace, Interior, and Conjugate Gradient Method for Large-Scale Bound-Constrained Minimization Problems, SIAM J. Sci. Comp. 21 (1) (1999) 1–23.

[15] T. F. Coleman, Y. Li, A reflective Newton method for minimizing a quadratic function subject to bounds on some of the variables, Tech. Rep. TR 92–1315, Department of Computer Science, Cornell University (1992).

[16] T. F. Coleman, Y. Li, On the convergence of reflective Newton methods for large-scale nonlinear minimization subject to bounds, Math. Programming 67 (1994) 189–224.

[17] T. F. Coleman, Y. Li, A Reflective Newton Method for Minimizing a Quadratic Function Subject to Bounds on Some of the Variables, SIAM J. Optimization 6 (4) (1996) 1040–1058.

[18] T. F. Coleman, Y. Li, An interior trust region approach for nonlinear minimization subject to bounds, SIAM J. Optimization 6 (2) (1996) 418–445.
[19] T. F. Coleman, M. A. Branch, A. Grace, Optimization Toolbox for Use with Matlab, The Math Works Inc., 1999.
[20] A. R. Conn, N. I. M. Gould, P. L. Toint, Trust-region methods, Society for Industrial and Applied Mathematics, Philadelphia, PA, USA, 2000.